Measurement, Evaluation and Analysis of Wall Thickness of 3D Airway Trees across Bifurcations ⋆

Xiaomin Liu[1] ⋆⋆, Danny Z. Chen[1], Merryn Tawhai[2], Eric Hoffman[3], and Milan Sonka[3]

[1] Department of Computer Science & Engineering, University of Notre Dame, USA
xliu9@nd.edu
[2] Auckland Bioengineering Institute, The University of Auckland, New Zealand
[3] Iowa Institute for Biomedical Imaging, The University of Iowa, USA
milan-sonka@uiowa.edu

Abstract. Airway segmentation and analysis is an essential step in the understanding of pulmonary anatomy and early detection of lung diseases. In this paper, we evaluate a newly developed method for segmenting the inner and outer surfaces of the airway tree. This is the first approach reported to validate the segmentation of the double wall surfaces for the entire airway tree including bifurcations. Two approaches help analyze the tree topology: (1) 3D thinning algorithm which produces a one-voxel wide centerline, and (2) Delaunay triangulation based generation of both the inner and outer 3D medial axes (sheets). The two airway wall surfaces are identified using a 3D optimal graph search approach. Once segmented, the bifurcation/carina areas are defined based on (1) the surface point proximity to the branch points identified on the centerline, and (2) the surface point distance from the 3D outer medial sheets. The wall thickness measurements for both the bifurcation/ non-bifurcation and carina/non-carina points are grouped and reported as a function of tree generation. The accuracy of wall thickness measurement is assessed on CT-scanned double-wall physical phantoms. The airway wall thickness accuracy is similar for the bifurcation/carina and non-bifurcation/carina areas. The measurements on normal human *in vivo* data reflect reasonable and consistent differences of wall thickness from generation to generation.

1 Introduction

Measurements of airway dimensions such as the local diameters and airway wall thickness provide important information contributing to the understanding of lung pathology and early detection of lung diseases. For instance, airway wall

⋆ This research was supported in part by NSF grants CCF-0515203 and CCF-0916606 and NIH grants R01-EB004640 and R01-HL064368.
⋆⋆ The work of this author was supported in part by a graduate fellowship from the Center for Applied Mathematics, University of Notre Dame.

thickening is inversely related to the degree of airflow obstruction [1], and attenuates airway reactivity in patients with asthma [2]. However, while a number of segmentation and evaluation methods have been proposed for automatically segmenting and measuring the airway inner surface [3–5], few methods are known for segmentation of the airway outer surface and the measurement of wall thickness. This is especially true for measurement of wall thickness across airway tree bifurcations. In [6], the airway outer surface was segmented by locally deforming the lumen mesh under specific force constraints. However, the optimality of the solution is not guaranteed.

Li *et al.* [7] extended a graph search based approach of Wu and Chen [8] to segmenting multiple interrelated surfaces together, and successfully applied it to the segmentation of 3D airway double surfaces on the non-branching part. The solution of the graph search is optimal with respect to given cost functions. As a further extension, a new method was recently developed by Liu *et al.* [9] to identify both the inner and outer surfaces of the entire intrathoracic airway tree in 3D including the bifurcations. While the visual assessment of the inner/outer wall segmentation in *in-vivo* data suggested that the double surfaces are captured well by the method, quantitative validation of the segmentation accuracy remained a challenging problem. Manual tracing of airway tree wall surfaces is very hard to obtain in completeness, and even if attempted, suffers from low reproducibility and high inter- and intra-observer variability due to image ambiguity of the outer surface.

Because of the topological complexity, airway bifurcations are the most difficult area for accurate segmentation and measurement. It is also of clinical importance to improve assessment accuracy on these areas. For example, the experimentally observed local accumulations of particles within bronchial airway bifurcations may play a crucial role in lung cancer induction [10]. The complete bifurcation should be able to cover the entire "Y" shaped part that connects to the relatively straight branches (which are the non-bifurcation areas). In addition, it is physiologically and maybe diagnostically interesting to focus on specific parts of the bifurcation, such as the carina area between two sub-branches. For example, widening and distortion of the carina is a serious sign because it usually indicates carcinoma of the lymph nodes around the region where the trachea divides [11]. A good validation method should be able to distinguish the bifurcation/carina and non-bifurcation/carina areas in the airway trees, and evaluate the results separately in both these areas.

To cope with the above difficulties, we perform extensive validation using a CT-scanned double surface bifurcating phantom with known wall thickness to optimize the cost function of graph search [9]. Then the segmentation method in [9] (with the optimized cost functions) is applied to human *in vivo* CT data. The wall thickness is analyzed as a function of generation. In order to do so, we employ two methods to identify the bifurcation and carina areas on the airway tree based on the one voxel wide 3D skeleton and 3D medial axis sheets, respectively. Then, the wall thickness is measured on the identified bifurcation/non-bifurcation and carina/non-carina points, grouped and compared for different

generations. Consequently, meaningful information is produced about the variability and consistency of wall thickness across normal subjects for individual generations of the airway trees.

2 Segmentation

The multi-layer optimal graph search based algorithm is employed to segment both the inner and outer airway walls as an entire tree [9]. The method can be outlined as follows (see [9] for full details):

(1) Pre-segmentation. A pre-segmentation is needed to provide the basic information about the object's global structure. It is not necessary for the pre-segmentation to be locally accurate. However, it is crucial to preserve the topology of the target object. In our experiments, the airway trees are pre-segmented using commercially available Pulmonary Workstation PW+ software (VIDA Diagnostics, Oakdale, IA). Once a labeled image is generated by the pre-segmentation, it is transformed into a triangulated mesh using the marching cube algorithm.

(2) Image resampling. Based on the outcome of the pre-segmentation, the image is resampled on each vertex of the initial surface mesh, resulting in a set of vectors (called *columns*) of voxels. 3D medial axes (sheets) are computed based on Voronoi diagrams, which help to determine the directions and lengths of the resampling columns.

(3) Graph construction. Each voxel in the columns is considered as a node in the graph. There are three types of edges, representing the relations of voxels within the same surface or between different surfaces. A cost function is assigned to each node combining the first and second derivative. To distinguish properties of the inner and outer surfaces, two inversely oriented Sobel operators are applied to capture the directional information of the intensity changes.

(4) Graph search. A minimum s-t cut algorithm [8, 7] is applied to the resulting graph to simultaneously search for the inner and outer surfaces of airway walls simultaneously. This graph search identifies double wall surfaces simultaneously for all branches and all bifurcations of the entire tree in a single optimization process.

3 Identification of airway bifurcation

Starting from the trachea, the airway splits into left and right main bronchi, and continues to decrease size in ever-smaller branches at each bifurcation. The resulting tree structure consists of several generations. The segmentation around the bifurcation is especially difficult task because of the topological complexity. The advantage of the algorithm in [9] is the ability to segment the double surfaces around the bifurcation as described above. To evaluate the segmentation and wall thickness measurement for the bifurcation regions, the bifurcation areas

and other tree segments must be identified to allow performance comparisons in these two areas. 3D skeleton/medial axis is a powerful approach to provide a simplified structure of the object which would capture the same topology of the original object, and thus provide the information about the branching points, tree segment generation, etc.

3.1 3D thinning

Airway tree skeleton is obtained using a 3D thinning algorithm presented by Lee [12]. (See Fig. 1) The algorithm iteratively deletes the simple points while preserving the topology (connectivity, the same number of holes and cavities in the object). The output of the thinning algorithm is a one-voxel wide centerline. A tree-labeling process follows using the centerline that identifies the branching and non-branching points using a depth-first-search (DFS). Both branching and non-branching points are associated with a number representing the generation.

Fig. 1. 3D skeleton of an airway tree colored according to tree generations.

The bifurcations are identified by using spheres centered at each branching point. The sphere diameters are proportional to the local branch diameter. In Fig. 2, the diameter of the sphere is twice as large as the local diameter in order to include the entire bifurcation. In this situation, some of the branches in the 3^{rd}, 4-6^{th} generations that are short (comparing to the local diameter) may become mostly included in the bifurcation (covered in red).

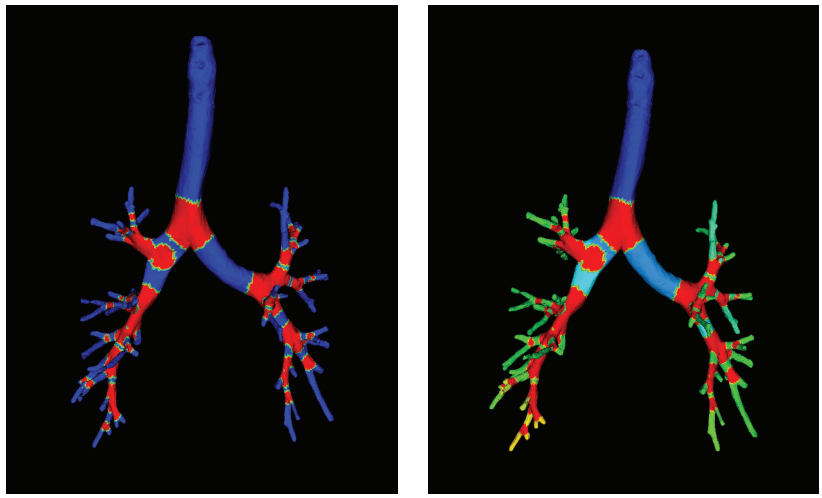

(a) (b)

Fig. 2. Airway trees with identified bifurcation and non-bifurcation areas. (a) Bifurcation areas are colored in red. (b) In this panel, bifurcation areas are colored in red while non-bifurcation areas are colored by generation.

As a well known phenomenon, the skeleton/medial axis is sensitive to local changes, which may cause undesirable fake branches in the skeleton. To get rid of these fake branches, we measured the length of each branch after the branching points are identified. Then, the branches that are short compared to local diameter are pruned out.

3.2 3D medial axis

3D thinning allows fast computation of the medial axis as it iteratively deletes all the surface points until a one-voxel wide centerline remains. Nevertheless, it lacks the ability to produce the outer medial axis, which may be important for capturing the changes in tree structure. While an approach based on Delaunay triangulation and Voronoi diagram of the surface may suffer from low computational efficiency, it produces both the inner and outer medial axis of the object at the same time and was chosen here.

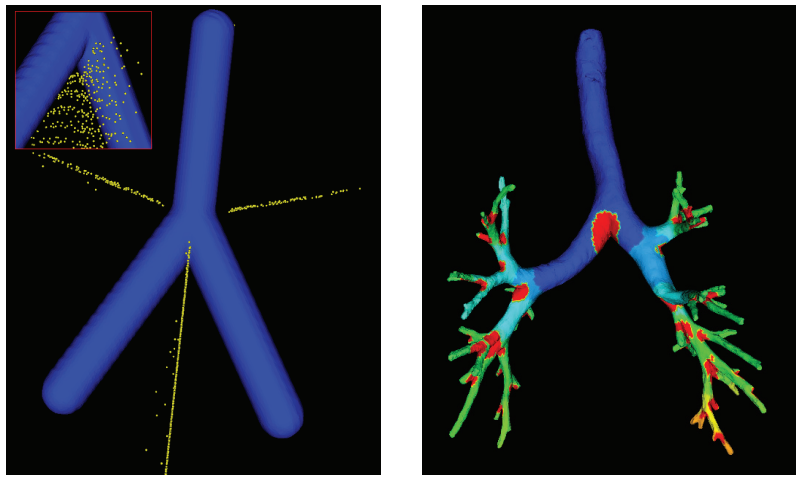

(a) (b)

Fig. 3. Carina regions consist of points that are close to the outer medial axis. (a) Outer medial axis points (yellow) around a bifurcation – detail shown in the upper left corner. (b) Red areas represent carina regions. The tree is labeled with different colors for different generations.

The output of the graph search segmentation is a triangulated surface, where neighboring vertices/points are connected by edges. We can compute the Voronoi diagram and the dual Delaunay triangulation of S in 3D [13]. The medial axis is computed by using the poles in the Delaunay triangulation, which are selected from the centers of the big Delaunay balls adjacent to vertices. A pole is assigned to each of the mesh vertices by selecting the largest pole among the vertex k-nearest neighbors, in order to reduce the impact of possible noise on the surface [13].

Surface points that are close to the outer medial axis are selected. For an object with tree-like structure such as the airway, parental generations always split into two child airways at the site of bifurcation. The area where the two child airways separate forms a V-shape, which is the difficult region for wall thickness measurement because of local topological changes. In anatomy, the tracheal carina is a cartilage-rich saddle region within the trachea that separates the two mainstem bronchi. We define the carina regions in our measurements as the saddle areas where each generation branches into two child generations. As illustrated in Fig. 3, the carina regions can be well represented by points that are within a small distance from the outer medial axis (once such distance is determined properly by the local diameter). By selecting different cut-off values, the carina regions are not necessarily part of the bifurcation areas as defined in the last section.

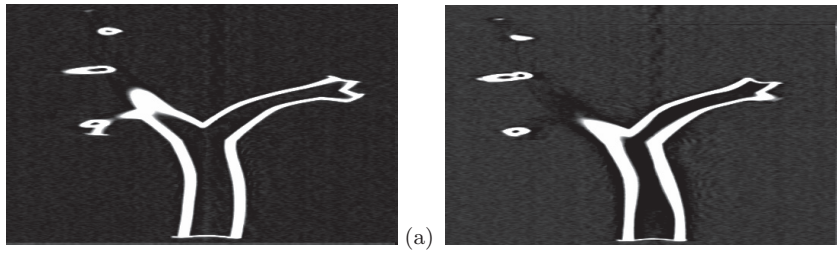

(a) (b)

Fig. 4. Example 2D slices from two CT scans of the double-wall phantoms. (a) Phantom with smooth wall thickness distribution. (b) Phantom with non-smooth wall thickness distribution.

4 Experimental methods and results

4.1 Evaluation based on bifurcation and carina identification

After the labeling of the airway tree and identification of bifurcation and carina areas, we measure the wall thickness for the entire tree and group the results according to different generations in both bifurcation/non-bifurcation and carina/non-carina areas. The thickness is measured between the two segmented surfaces along the normal direction to the inner surface. The evaluation has been performed on two kinds of data: (1) two double-wall bifurcating phantoms derived from human *in vivo* data with smooth and non-smooth wall thickness, and (2) *in vivo* human CT scans.

Double wall phantoms The evaluation of wall thickness measurement is first performed on CT scans of two double wall phantoms with predefined wall thickness (Fig. 4). To construct the phantom, segmented volumetric images from multi-detector row computed tomography scanning of a healthy male lung are imported into the cmgui visualization software (www.cmiss.org). A bi-cubic Hermite finite element mesh is geometry-fitted to the surface of the outer wall. The mesh is given a volume by defining a wall thickness at each mesh node. The phantom is manufactured using a solid 3D printer (the Dimension Elite 3D Printer). The solid structure is composited of 0.254 mm thick layers of ABS plastic and support material. The support material is dissolved following manufacturing. The resolution of the discretized tetrahedral mesh is set at three levels as indicated in the results. The smooth and non-smooth phantoms have identical outer wall surfaces. The only difference in their geometry is the wall thickness at the mesh nodes and the derivatives for inner surface curvature. The inner surface derivatives in the non-smooth phantom are modified arbitrarily to create a challenging structure on which to test the algorithm. The wall thickness of both bifurcation and non-bifurcation areas is calculated and listed in the following table. The image size is $512 \times 512 \times 313$ and the voxel size is $0.23 \times 0.23 \times 0.7\text{mm}^3$.

The ground truth of the wall thickness is computed from the original digital mesh of the double wall phantom that is used for the fast prototyping of the

Table 1. Mean wall thickness errors for a double-surface bifurcating smooth phantom.

Smooth (mm)	Number of points	Unsigned error average(mm)	Signed error(mm)
Coarse	10374	0.27 ± 0.23	-0.023 ± 0.35
Original	40743	0.27 ± 0.23	-0.025 ± 0.35
Fine	73119	0.27 ± 0.23	-0.022 ± 0.35

Table 2. Mean wall thickness errors for a double-surface bifurcating non-smooth phantom.

Nonsmooth (mm)	Number of points	Unsigned error average(mm)	Signed error(mm)
Coarse	11891	0.27 ± 0.22	-0.000 ± 0.35
Original	46537	0.27 ± 0.22	-0.001 ± 0.35
Fine	83800	0.27 ± 0.22	-0.004 ± 0.35

physical phantom. The mesh is then down-sampled to form a coarse mesh that is half as dense as the original one, and also up-sampled to a fine mesh twice as dense as the original one. As summarized in Tables 1 and 2, the mean errors and standard deviations of the wall thickness measurement are low (subvoxel) for both the smooth and non-smooth phantoms and thus do not depend on the mesh density. When considering the branching and non-branching areas on the phantom, the average errors and standard deviations of the wall thickness measurement are determined and shown in Fig. 5.

Human *in vivo* data The double-wall airway tree segmentation method is used to determine airway wall thickness for 7 sets of human CT scans from 7 normal subjects. The image size varies from $512 \times 512 \times 464$ to $512 \times 512 \times 587$, and the voxel size is $0.59 \times 0.59 \times 0.60\text{mm}^3$.

Fig. 6 (a) shows the average wall thickness at the bifurcation and non-bifurcation areas measured and grouped by airway tree generations. Fig. 6 (b) shows the wall thickness of the carina and non-carina areas, also as a function of generations. These figures depict a similar trend of the wall thickness, decreasing from the first to the sixth generation, that is consistent with the generational decrease of the local diameter. For the seventh to eleventh generations where the airway wall is relatively thin, wall thickness seems to stop decreasing. Comparing the measurements in the bifurcation and carina areas, we can see that the wall thickness of the bifurcation is larger than the wall thickness of the carina for the first six generations. The average wall thickness of the carina area is also smaller than non-carina area for the first a few generations. The measurements in the bifurcation and carina areas are very similar after the sixth generation.

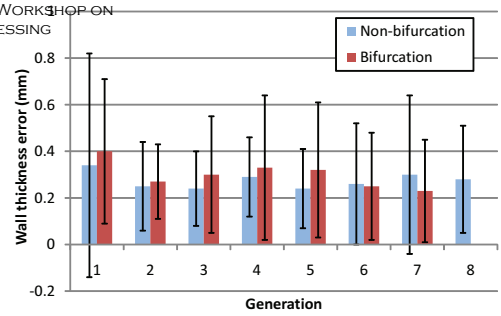

(a)

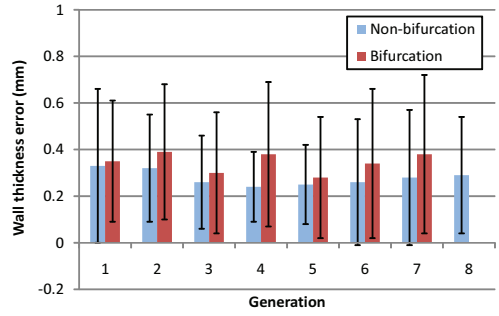

(b)

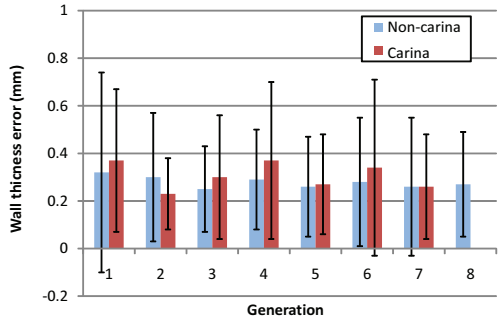

(c)

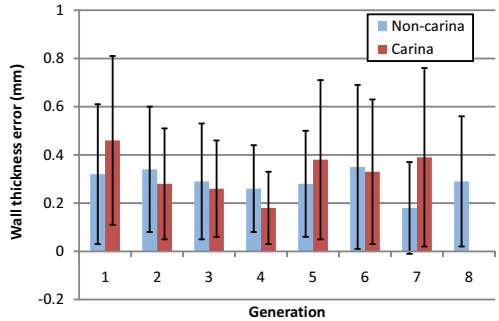

(d)

Fig. 5. The wall thickness measurement for the double-wall phantoms. The average errors and standard deviations are calculated for: (a) Bifurcation/non-bifurcation areas of the smooth phantom; (b) Bifurcation/non-bifurcation area of the non-smooth phantom; (c) Carina/non-carina areas of the smooth phantom; (d) Carina/non-carina areas of the non-smooth phantom.

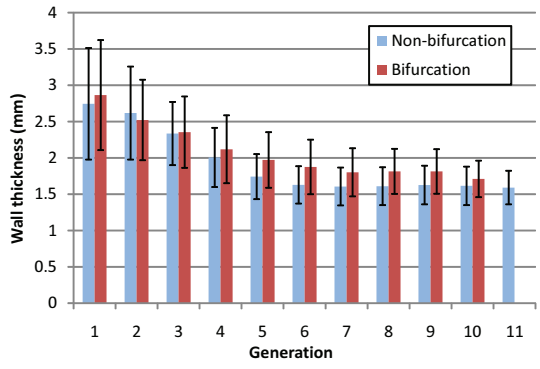

(a)

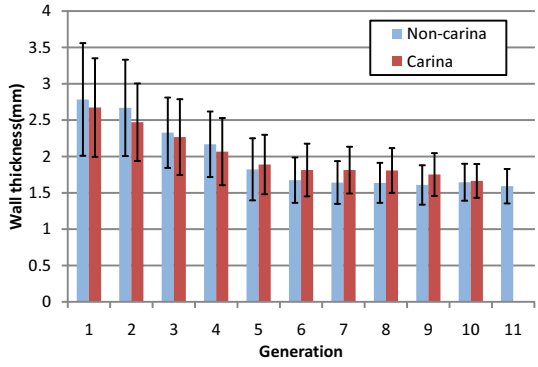

(b)

Fig. 6. Wall thickness as a function of airway tree generation. (a) Average wall thickness in bifurcation/non-bifurcation areas. (b) Average wall thickness in carina/non-carina areas. Error bars depict standard deviations.

5 Discussion and conclusion

An evaluation method of the double-surface airway tree segmentation is presented that simultaneously determines inner and outer surfaces of all branches and bifurcations for the entire tree. The surface points have been labeled with different generation automatically according to the skeleton. The complete bifurcation and relatively smaller carina area have been defined using two different methods of extracting the 3D medial axes/skeleton of the airway tree. By applying graph search based segmentation approaches, the experimental results on both the bifurcation/non-bifurcation and carina/non-carina areas achieve subvoxel accuracy in physical double-wall phantoms. The wall thickness analysis in the human *in vivo* data shows consistent decrease of mean wall thickness and standard deviation from parent to child generations. The proposed evaluation method is the first to allow separate measurement of airway wall thickness in the bifurcation and carina regions of the airway trees using a globally optimal

approach. Therefore, the reported method provides a new way for analyzing the airway wall properties in bifurcating regions. The quantification of wall properties in bifurcations allows novel disease-specific studies of intrathoracic airway tree physiology and function.

References

1. Deveci, F., Murat, A., Turgut, T., Altunta, E., Muz, M.H.: Airway wall thickness in patients with COPD and healthy current smokers and healthy non-smokers: assessment with high resolution computed tomographic scanning. Respiration **71** (2004) 602–610
2. Niimi, A., Matsumoto, H., Takemura, M., Ueda, T., Chin, K., Mishima, M.: Relationship of airway wall thickness to airway sensitivity and airway reactivity in asthma. American Journal of Respiratory and Critical Care Medicine **168** (2003) 983–988
3. Aykac, D., Hoffman, E.A., McLennan, G., Reinhardt, J.M.: Segmentation and analysis of the human airway tree from three-dimensional X-ray CT images. IEEE Transaction On Medical Imaging **22** (2003) 940–950
4. Fetita, C.I., Preteux, F., Beigelman-Aubry, C., Grenier, P.: Pulmonary airways: 3-D reconstruction from multislice CT and clinical investigation. IEEE Transaction on Medical Imaging **23** (2004) 1353–1364
5. Tschirren, J., Hoffman, E.A., McLennan, G., Sonka, M.: Intrathoracic airway trees: Segmentation and airway morphology analysis from low-dose CT scans. IEEE Transaction on Medical Imaging **24** (2005) 1529–1539
6. Saragaglia, A., Fetita, C., Brillet, P.Y., Preteux, F., Grenier, P.A.: Airway wall thickness assessment: A new functionality in virtual bronchoscopy investigation. In Manduca, A., Hu, X.P., eds.: Proc. of SPIE Medical Imaging 2007: Physiology, Function, and Structure from Medical Images. Volume 6511. (2007) 65110P
7. Li, K., Wu, X., Chen, D.Z., Sonka, M.: Optimal surface segmentation in volumetric images - A graph-theoretic approach. IEEE Transactions on Pattern Analysis and Machine Intelligence **28** (2006) 119–134
8. Wu, X., Chen, D.Z.: Optimal net surface problems with applications. In: Widmayer, P., Triguero, F., Morales, R., Hennessy, M., Eidenbenz, S., Conejo, R. (eds.) ICALP 2002. LNCS. (2002) 1029–1042
9. Liu, X., Chen, D.Z., Wu, X., Sonka, M.: Optimal graph search based image segmentation for objects with complex topologies. In Pluim, J.P., Dawant, B.M., eds.: Proc. of SPIE Medical Imaging 2009: Image Processing. Volume 7259. (2009) 725915
10. Balashazy, I., Hofmann, W., Heistracher, T.: Local particle deposition patterns may play a key role in the development of lung cancer. Journal of Applied Physiology **94** (2003) 1719–1725
11. Ellis, H.: Clinical anatomy: A revision and applied anatomy for clinical students. tenth edn. Blackwell (2002)
12. Lee, T.C., Kashyap, R.L., Chu, C.N.: Building skeleton models via 3-D medial surface/axis thinning algorithms. Computer Vision, Graphics, and Image Processing **56** (1994) 462–478
13. Dey, T.K., Sun, J.: Normal and feature estimations from noisy point clouds. Technical Report OSU-CISRC-7/50-TR50 (2005)